

# Extension of dynamical mean-field theory by inclusion of nonlocal two-site correlations with variable distance

Torben Jabben and Norbert Grewe

*Institut für Festkörperphysik, Technische Universität Darmstadt, Hochschulstr. 8, 64289 Darmstadt, Germany*

Sebastian Schmitt\*

*Lehrstuhl für Theoretische Physik II, Technische Universität Dortmund, Otto-Hahn-Str. 4, 44221 Dortmund, Germany*

(Dated: October 30, 2018)

We present a novel approximation scheme for the treatment of strongly correlated electrons in arbitrary crystal lattices. The approach extends the well-known dynamical mean field theory to include nonlocal two-site correlations of arbitrary spatial extent. We extract the nonlocal correlation functions from two-impurity Anderson models where the impurity-impurity distance defines the spatial extent of the correlations included. Translational invariance is fully respected by our approach since correlation functions of any two-impurity cluster are periodically embedded to  $k$ -space via a Fourier transform. As a first application, we study the two-dimensional Hubbard model on a simple-cubic lattice. We demonstrate how pseudogap formation in the many-body resonance at the Fermi level results from the inclusion of nonlocal correlations. A comparison of the spectral function with the dynamical-cluster approximation shows qualitative agreement of high- as well as low-energy features.

PACS numbers: 71.10.-w, 74.72.Kf, 05.10.-a, 02.70.-c

## I. INTRODUCTION

Compounds with strongly correlated electrons<sup>1,2</sup> are in the focus of modern solid-state research. They usually contain transition metal ions where part of the valence electrons move in narrow bands or are nearly localized. Prominent examples include high-temperature cuprate superconductors,<sup>3</sup> frustrated magnets<sup>4</sup> and heavy-fermion systems.<sup>5</sup>

Despite a large effort, various fundamental questions are still open.<sup>2,5-7</sup> The model system of a single transition metal ion immersed into a metallic matrix has essentially been solved by analytical<sup>8,9</sup> and powerful numerical methods.<sup>10,11</sup> However, the more general case of regular crystal lattices with strong electron correlations in or near a metallic regime is much more difficult to handle. The large number of relevant electronic states and the interplay of hybridization and interaction effects makes it even difficult to identify relevant degrees of freedom or arrive at low-energy effective models.

An understanding of electronic correlations lies at the heart of most open problems in this field. Although the metallic character of many materials lends hope to the hypothesis that relevant interactions are screened and thus of short range, they can in principle drive correlations over all ranges of spatial distances.

Modern approaches<sup>12</sup> focused on the dominant role of the local Coulomb repulsion. In particular, dynamical mean-field theory<sup>13</sup> (DMFT) has proven to be very successful. It is capable of describing lattice versions of the Kondo effect in a regime of sizable local magnetic moments and provides valuable insights to the correlation driven Mott-Hubbard metal-to-insulator transition.<sup>14</sup> These approximations have met with considerable success concerning, for example, one-particle

properties<sup>15,16</sup> or susceptibilities.<sup>17</sup>

However, many phenomena require the inclusion of nonlocal correlations. Prominent examples are systems near a quantum critical point<sup>18</sup> or cuprate high-temperature superconductors.<sup>3</sup> In recent years extensions of DMFT have been put forward to remedy these shortcomings by the inclusion of some spatial correlations between electrons.<sup>19</sup> In the cluster approaches, the problem is mapped to an effective cluster of few lattice sites and, in analogy to DMFT, this cluster is treated like a complex impurity in a dynamic external field.

These approaches capture short-range correlations quite accurately and have contributed considerably to the understanding of pseudogaps and shadow bands,<sup>6,20-22</sup> as well as to the possible occurrence of quantum critical points.<sup>23,24</sup>

However, some problems remain in these theories. In cluster DMFT<sup>25</sup> (CDMFT), for example, the translational invariance of the crystal lattice is not fully respected. The dynamical cluster approximation<sup>26</sup> (DCA) remedies this shortcoming, but the question remains which choice for the size and geometry of the cluster is advantageous.<sup>27</sup> But the most fundamental limitation is the restriction to rather short-ranged correlations.

In this paper we present a novel kind of self-consistent approach to correlated lattice systems which is in principle capable of including nonlocal correlations of arbitrary distance. It extends the well-known DMFT by the inclusion of two-site correlations of all length-scales and is thus termed *nonlocal DMFT* (NLD). These correlations are incorporated by a mapping of the lattice model onto a multitude of two-impurity Anderson models (TIAM), where the impurity-impurity distance is varied. The translational invariance and crystal symmetries are fully respected by the scheme proposed here.

The details of the mapping between lattice and two-impurity models is presented in Sec. II. As a first application we study in Sec. III the two-dimensional Hubbard model on a square lattice, a model which is usually considered in connection with cuprate superconductors. We utilize the recently developed two-impurity enhanced noncrossing approximation<sup>28</sup> as the two-impurity solver and analyze the results obtained with respect to the quality of our novel lattice approach and to their physical implications. A short conclusion and outlook is given in Sec. IV.

## II. SELF-CONSISTENT LATTICE THEORY

In order to introduce the ideas underlying our self-consistent scheme we restrict the following discussion to the example of a single-band Hubbard model

$$\hat{H} = \sum_{\underline{k}, \sigma} (\epsilon + t_{\underline{k}}) \hat{c}_{\underline{k}, \sigma}^\dagger \hat{c}_{\underline{k}, \sigma} + U \sum_j \hat{n}_{j, \uparrow} \hat{n}_{j, \downarrow}. \quad (1)$$

We use a mixed representation, where the kinetic energy is expressed in terms of band states with momentum  $\underline{k}$  and spin  $\sigma = \{+, -\} = \{\uparrow, \downarrow\}$  which are created (annihilated) by the operators  $\hat{c}_{\underline{k}, \sigma}^\dagger$  ( $\hat{c}_{\underline{k}, \sigma}$ ).  $\epsilon$  denotes the local single-particle energy and the dispersion  $t_{\underline{k}}$  is the Fourier transformation of the hopping matrix elements  $t_{ij}$  between lattice sites  $i$  and  $j$  with lattice vectors  $\underline{R}_i$  and  $\underline{R}_j$ , respectively. The lattice structure, i.e. the type of lattice and topology of the hopping matrix elements, is completely encoded into the dispersion relation  $t_{\underline{k}}$ . The interaction energy characterized by the Coulomb matrix element  $U$  is conveniently written in terms of local occupation number operators  $\hat{n}_{j, \sigma} = \hat{c}_{j, \sigma}^\dagger \hat{c}_{j, \sigma}$  which measure an electron on site  $j$  with spin  $\sigma$ . The lattice constant  $a = 1$  will serve as the fundamental length scale and the spin index  $\sigma$  will be dropped whenever possible without ambiguities.

The extension of the novel approach presented here to more general systems with multiple bands and/or more complicated interactions can be readily obtained.

The fundamental quantity of interest is the one-particle Green function which obeys the Dyson equation

$$G_{\underline{k}}(z) = g_{\underline{k}}(z) + g_{\underline{k}}(z)t_{\underline{k}}(z)G_{\underline{k}}(z) \quad (2)$$

which is represented graphically in Fig. 1. The formal solution is given by

$$G_{\underline{k}}(z) = [g_{\underline{k}}(z)^{-1} - t_{\underline{k}}]^{-1}. \quad (3)$$

The correlated part

$$g_{\underline{k}}(z) = [z - \epsilon - \Sigma_{\underline{k}}(z)]^{-1} \quad (4)$$

incorporates the irreducible self-energy  $\Sigma_{\underline{k}}(z)$  and accounts for the correction to the noninteracting system due to the interaction term proportional to  $U$  in

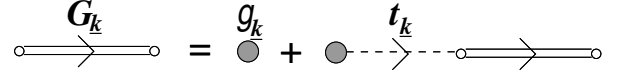


FIG. 1. Diagrammatic representation of Eq. (2).

the Hamiltonian Eq. (1). It describes the interaction-induced, i.e. correlated, part of the propagation process, in which single-particle transfers via elementary hoppings are excluded.

It is useful to re-write the Dyson equation (2) in terms of the lattice  $T$ -matrix  $T_{\underline{k}}$ ,

$$G_{\underline{k}}(z) = g_{\underline{k}}(z) + g_{\underline{k}}(z)T_{\underline{k}}(z)g_{\underline{k}}(z), \quad (5)$$

which is commonly defined via

$$T_{\underline{k}}(z) = t_{\underline{k}} + t_{\underline{k}}G_{\underline{k}}(z)t_{\underline{k}} \quad (6)$$

$$= \frac{t_{\underline{k}}}{1 - g_{\underline{k}}(z)t_{\underline{k}}}. \quad (7)$$

In the last equality the explicit form of Eq. (3) is used.

Processes contributing to the irreducible self-energy  $\Sigma_{\underline{k}}(z)$  can be grouped together according to the nature and degree of correlations they contain. One contribution represents the exact solution of an isolated interacting local site, which is represented by the “atomic” self-energy<sup>29</sup>  $\tilde{\Sigma}^{(0)}(z) = U \frac{(z - \epsilon)(1 - \langle \hat{n}_\sigma \rangle)}{z - \epsilon - U \langle \hat{n}_\sigma \rangle}$ . All other terms incorporate genuine lattice processes. Some of these are captured by the well-known self-energy of the DMFT-approximation, which furnishes a  $\underline{k}$ -independent but dynamic contribution  $\tilde{\Sigma}^{(1)}(z)$ . It incorporates loops through the lattice attached at one site at which all local (dynamic) correlations are fully respected. Beyond DMFT, correlations between two or more of these loops are generated by interaction events at different sites and thus constitute nonlocal cumulant corrections.

Organizing these cumulant corrections according to the number of different lattice sites they correlate, the correlation function of Eq. (4) can be expanded as

$$g_{\underline{k}}^{-1}(z) = z - \epsilon - \tilde{\Sigma}^{(0)}(z) - \tilde{\Sigma}^{(1)}(z) - \tilde{\Sigma}_{\underline{k}}^{(2)}(z) - \tilde{\Sigma}_{\underline{k}}^{(3)}(z) - \dots \quad (8)$$

It is the aim of the present investigation to identify and calculate the self-energy contribution  $\tilde{\Sigma}_{\underline{k}}^{(2)}(z)$ , which contains all nonlocal correlations between any two sites of the lattice. While two-site correlations are thus explicitly included in this scheme, three-site and higher-order nonlocal cumulant corrections  $\tilde{\Sigma}_{\underline{k}}^{(n)}(z)$  with  $n \geq 3$  are neglected. The function incorporating these correlations,  $g_{\underline{k}}(z)$ , will be extracted from solutions of various two-impurity models where the impurity-impurity distance is varied. Then, the Dyson equation (2), respectively its solution Eq. (3), is used to obtain the lattice Green function.

### A. Mapping between the lattice and a set of two-impurity models

In order to extract the function  $g_{\underline{k}}(z)$  which includes two-site correlations, we consider a two-impurity Anderson model<sup>30</sup> (TIAM). The two magnetic impurities are immersed with finite distance into a host with a noninteracting conduction band. The Hamiltonian of one such general TIAM with a fixed distance vector  $\underline{a}$  is given by

$$\begin{aligned} \hat{H}^{(2\text{imp},\underline{a})} = & \sum_{j=\{1,2\},\sigma} \epsilon_j \hat{c}_{j,\sigma}^\dagger \hat{c}_{j,\sigma} + \sum_{j,l,\sigma,\sigma'} U_{jl}^{(\underline{a})} \hat{n}_{j,\sigma} \hat{n}_{l,\sigma'} \quad (9) \\ & + \sum_{j,\sigma} t_{jl}^{(\underline{a})} \hat{c}_{j,\sigma}^\dagger \hat{c}_{l,\sigma} + \sum_{j,l} \hat{W}_{jl}^{(\underline{a})} \\ & + \sum_{\underline{k},\sigma} \epsilon_{\underline{k}} \hat{a}_{\underline{k},\sigma}^\dagger \hat{a}_{\underline{k},\sigma} \\ & + \frac{1}{\sqrt{N}} \sum_{\underline{k},j,\sigma} (V_{\underline{k}} e^{-i\underline{k}\cdot\underline{R}_j} \hat{a}_{\underline{k},\sigma}^\dagger \hat{c}_{j,\sigma} + h.c.). \end{aligned}$$

The  $\hat{c}$ -operators ( $\hat{a}$ -operators) describe local interacting electrons on the impurities at positions  $\underline{R}_j \in \{\underline{R}_1, \underline{R}_2\}$  (the noninteracting conduction band electrons with momentum  $\underline{k}$ ) with spin  $\sigma$ . The spatial distance between the two impurities is fixed and given by  $\underline{a} = \underline{R}_1 - \underline{R}_2$ .  $\epsilon_j$  is the local single-particle energy on each impurity site and  $U_{jl}^{(\underline{a})}$  are the Coulomb matrix elements of the local ( $j = l$ ) and nonlocal ( $j \neq l$ ) density-density interactions. The term proportional to  $t_{jl}^{(\underline{a})}$  is a possible direct single-particle hopping inside the two-impurity cluster and  $\hat{W}_{jl}^{(\underline{a})}$  collects additional interactions as, for example, exchange, pair hopping or correlated hopping. The last term represents the hybridization between interacting electrons of the two-site cluster and noninteracting band electrons.

The scheme proposed is capable of properly treating all such terms in the Hamiltonian so that nonlocal Coulomb interaction or long-ranged single-particle hopping matrix elements can in principle be considered. For the present case of the single-band Hubbard model nonlocal Coulomb matrix elements are not included and the single-particle hopping coincides with that of the underlying lattice as specified in the Hamiltonian of Eq. (1).

Since we are only interested in properties of the interacting  $c$ -electrons neither the hybridization matrix elements nor the dispersion  $\epsilon_{\underline{k}}$  of the band electrons are directly of interest. Only the effective medium for the two-impurity cluster is relevant which is expressed in terms of these parameters as

$$\tilde{T}_{\underline{a}}^{(2\text{imp},\underline{a})}(z) = \frac{1}{N} \sum_{\underline{k}} e^{-i\underline{k}\cdot\underline{a}} \frac{|V_{\underline{k}}|^2}{z - \epsilon_{\underline{k}}}. \quad (10)$$

It represents propagation processes via the noninteracting conduction band in form of irreducible loops starting and ending at the two-site cluster. In our truly

self-consistent theory for a lattice model a corresponding effective medium  $\tilde{T}_{\underline{a}}^{(2\text{imp},\underline{a})}$  has to be determined by an appropriate mapping between the lattice and the two-impurity model. Therefore, it becomes dressed and takes into account repeated interactions on local shells of other lattice sites.

A Dyson equation for the local two-impurity Green functions is set up as follows

$$\begin{aligned} \underline{\underline{G}}^{(2\text{imp},\underline{a})} = & \underline{\underline{g}}^{(2\text{imp},\underline{a})} \quad (11) \\ & + \underline{\underline{g}}^{(2\text{imp},\underline{a})} \left( \underline{\underline{t}}^{(\underline{a})} + \tilde{\underline{\underline{T}}}^{(2\text{imp},\underline{a})} \right) \underline{\underline{G}}^{(2\text{imp},\underline{a})}, \end{aligned}$$

where we used a matrix notation for the spatial components

$$\underline{\underline{A}}^{(2\text{imp},\underline{a})} = \begin{pmatrix} A_{\underline{0}}^{(2\text{imp},\underline{a})} & A_{\underline{a}}^{(2\text{imp},\underline{a})} \\ A_{-\underline{a}}^{(2\text{imp},\underline{a})} & A_{\underline{0}}^{(2\text{imp},\underline{a})} \end{pmatrix}. \quad (12)$$

The correlated part  $\underline{\underline{g}}^{(2\text{imp},\underline{a})}$  represents the cluster cumulant Green function and takes the interaction matrix elements into account. Therefore, the direct  $\sim \underline{\underline{t}}^{(\underline{a})}$  and indirect hopping events via the effective medium  $\sim \tilde{\underline{\underline{T}}}^{(2\text{imp},\underline{a})}$  are explicitly incorporated in Eq (11).

The Dyson equation (11) can be formally solved to yield

$$\underline{\underline{G}}^{(2\text{imp},\underline{a})}(z) = \left[ \underline{\underline{g}}^{(2\text{imp},\underline{a})}(z)^{-1} - \underline{\underline{t}}^{(\underline{a})} - \tilde{\underline{\underline{T}}}^{(2\text{imp},\underline{a})}(z) \right]^{-1}, \quad (13)$$

which apart from the matrix structure and the occurrence of the hopping matrix  $\underline{\underline{t}}^{(\underline{a})}$  has the same form as in the single-impurity case.<sup>9</sup>

It is instructive to formulate the above equations in terms of the full  $T$ -matrix of the TIAM, thereby establishing an equivalence to the lattice equations (5) to (7). The local Green function can be expressed as

$$\underline{\underline{G}}^{(2\text{imp},\underline{a})} = \underline{\underline{g}}^{(2\text{imp},\underline{a})} + \underline{\underline{g}}^{(2\text{imp},\underline{a})} \tilde{\underline{\underline{T}}}^{(2\text{imp},\underline{a})} \underline{\underline{g}}^{(2\text{imp},\underline{a})}. \quad (14)$$

In contrast to the irreducible medium  $\tilde{\underline{\underline{T}}}^{(2\text{imp},\underline{a})}$ , the  $T$ -matrix incorporates repeated visits of the two-impurity cluster. The  $T$ -matrix is thus built up from irreducible loops, accounted for by the inclusion of  $\underline{\underline{t}}^{(\underline{a})} + \tilde{\underline{\underline{T}}}^{(2\text{imp},\underline{a})}$  for steps inside and outside the cluster, and repeated dwellings inside the cluster, where each visit contributes a factor  $\underline{\underline{g}}^{(2\text{imp},\underline{a})}$ . It can be expressed as

$$\underline{\underline{T}}^{(2\text{imp},\underline{a})} = \left[ \left( \underline{\underline{t}}^{(\underline{a})} + \tilde{\underline{\underline{T}}}^{(2\text{imp},\underline{a})} \right)^{-1} - \underline{\underline{g}}^{(2\text{imp},\underline{a})} \right]^{-1}. \quad (15)$$

A mapping between the two-impurity and the lattice model is accomplished by connecting the irreducible correlation functions  $g_{\underline{a}}(z)$  of both approaches. For each nonzero distance vector  $\underline{a}$  with solution  $g_{\underline{a}}^{(2\text{imp},\underline{a})}(z)$  of the two-impurity model, we identify

$$g_{\underline{a}}(z) \stackrel{!}{=} \frac{1}{\nu_a} g_{\underline{a}}^{(2\text{imp},\underline{a})}(z) \quad (\underline{a} \neq \underline{0}) \quad (16)$$

where the matrix elements [cf. Eq. (12)]

$$g_{\underline{a}}(z) = \frac{1}{N} \sum_{\underline{k}} e^{-i\mathbf{k}\cdot\mathbf{a}} g_{\underline{k}}(z) \quad (17)$$

is the Fourier transform of the lattice correlation function of Eq. (4) and  $\nu_a$  the number sites which have a distance  $a = |\underline{a}| = \sqrt{\sum_i a_i^2}$  to a given site.

The prefactor of  $\frac{1}{\nu_a}$  in Eq. (16) arises due to the restricted phase-space for scattering in the two-impurity model compared to the lattice situation. In the two-impurity cluster the interaction-induced scattering always transfers the electron from one site to the other at distance  $\underline{a}$ . In contrast, in the lattice the scattering process transfers an electron only in a fraction  $\frac{1}{\nu_a}$  of cases to one specific site with distance  $a = |\underline{a}|$ .

There is some ambiguity for the correlation function with zero distance  $\underline{a} = \underline{0}$ . While in the lattice there is only one such function,  $g_{\underline{0}}(z)$ , there exist many such functions  $g_{\underline{0}}^{(2\text{imp},\underline{a})}$  from all the effective two-impurity models, one for each distance  $\underline{a}$ . Then the question arises, which of all these functions should be chosen. To this end, we take a constructive approach, where we start from a reference correlation function  $g^{\text{DMFT}}(z)$  obtained with the DMFT and add to it all additional correlations of representative two-impurity clusters at different distances

$$g_{\underline{0}}(z) = g^{\text{DMFT}}(z) + \sum_{|\underline{a}|} \left[ g_{\underline{0}}^{(2\text{imp},\underline{a})}(z) - g^{\text{DMFT}}(z) \right]. \quad (18)$$

The momentum dependent correlation function of the lattice theory is now given by the inverse Fourier transform

$$g_{\underline{k}}(z) = \sum_{\underline{a}} e^{i\mathbf{k}\cdot\mathbf{a}} g_{\underline{a}}(z) \quad (19)$$

which directly leads to the full lattice Green function via Eq. (3).

As explained after Eq (10), the effective medium  $\tilde{T}^{(2\text{imp},\underline{a})}$  in the framework of our self-consistent theory has to be obtained from lattice quantities. This is achieved by identifying the momentum dependent  $T$ -matrices of both models,

$$T_{\underline{k}}(z) \stackrel{!}{=} T_{\underline{k}}^{(2\text{imp})}(z) = \sum_{\underline{a}} e^{i\mathbf{k}\cdot\mathbf{a}} T_{\underline{a}}^{(2\text{imp},\underline{a})}(z). \quad (20)$$

The momentum dependent  $T$ -matrix  $T_{\underline{k}}$  incorporates the correct translationally invariant linear combination of two-site propagations with a fixed distance. Inverting the Fourier transform and using Eq. (7) we obtain the  $T$ -matrix for a two-impurity model with fixed distance  $\underline{a}$

$$T_{\underline{a}}^{(2\text{imp},\underline{a})} = \frac{1}{N} \sum_{\underline{k}} e^{-i\mathbf{k}\cdot\mathbf{a}} \frac{t_{\underline{k}}}{1 - g_{\underline{k}}(z)t_{\underline{k}}}. \quad (21)$$

From this the irreducible medium for the two impurity model can be obtained by inverting Eq. (15) and inserting the known expression for  $\underline{g}^{(2\text{imp},\underline{a})}$ .

Lattice and crystal symmetries are completely respected in the present approach. Lattice-translational invariance is incorporated by construction. Even though the two-impurity models are solved for distances in real-space, the correlation functions  $g_{\underline{a}}^{(2\text{imp},\underline{a})}(z)$ , which explicitly exclude single-particle hopping, can be periodized for this purpose with the help of a Fourier transform to yield the lattice correlation function  $g_{\underline{k}}(z)$ . Crystal symmetries are also fully respected since all the two-impurity models for which the distance vectors  $\underline{a}_i$  are generated by point-group transformations, have identical effective media and are therefore identical. Point group symmetries can even be used to decrease the computational cost as only one representative two-impurity model of such a group of symmetry-related points needs to be solved. The solutions of all the others follow by symmetry operations.

We conclude this section by summarizing the steps of the calculation scheme:

1. Chose a set of  $N_a$  representative distance vectors  $\{\underline{a}_i\}$  with  $i = 1, \dots, N_a$ , one for each set of symmetry-related distance vectors.
2. Start with an initial guess for the effective media  $\tilde{T}^{(2\text{imp},\underline{a}_i)}$  for each distance vector.
3. Solve  $N_a$  different effective two-impurity models, one for each representative distance  $\underline{a}_i$  with the medium  $\tilde{T}^{(2\text{imp},\underline{a}_i)}$ . The result are  $N_a$  (matrix) Green functions  $\underline{G}^{(2\text{imp},\underline{a}_i)}$  from which the correlation functions  $\underline{g}^{(2\text{imp},\underline{a}_i)}$  are derived via the inversion of Eq. (13),

$$\underline{g}^{(2\text{imp},\underline{a})} = \left[ \underline{G}^{(2\text{imp},\underline{a})-1} + \underline{t}^{(\underline{a})} + \tilde{T}^{(2\text{imp},\underline{a})} \right]^{-1}. \quad (22)$$

4. Map the correlation functions of the two-impurity models to their lattice counterparts for fixed distances with Eqs. (16) and (18). Fourier-transform these  $g_{\underline{a}_i}(z)$  via Eq. (19) to obtain  $g_{\underline{k}}(z)$ .
5. Use  $g_{\underline{k}}(z)$  and Eq. (21) to get the two-impurity  $T$ -matrix  $T_{\underline{a}_i}^{(2\text{imp},\underline{a}_i)}$  for each distance vector  $\underline{a}_i$ . A new guess for the effective medium  $\tilde{T}^{(2\text{imp},\underline{a}_i)}$  is obtained with the inversion of Eq. (15),

$$\underline{t}^{(\underline{a})} + \tilde{T}^{(2\text{imp},\underline{a})} = \left[ \underline{T}^{(2\text{imp},\underline{a})-1} + \underline{g}^{(2\text{imp},\underline{a})} \right]^{-1}. \quad (23)$$

6. Go back to step 3 and iterate until convergence is reached.

One-particle spectra of the lattice are then obtained from Eq. (3) in momentum space and the local function via a Fourier transform.

An earlier approach of Schiller and Ingersent also utilizes a two-impurity model to extend the DMFT to include nonlocal correlations.<sup>31</sup> However there are various differences to our approach. They consider an expansion in the inverse spatial dimension  $\frac{1}{d}$  and consequently employ the two-impurity model only for one specific distance, i.e. nearest-neighbor sites only. Additionally, they identify the irreducible self-energies [cf. Eq. (4)] of the lattice and the two-impurity model. In contrast, we establish the mapping between the lattice and the effective impurity models via the correlation function  $g_{\underline{a}}$ . This represents a crucial difference, since  $g_{\underline{a}}$  includes *all* propagation processes correlated between the two sites via the interaction. Thus, it also incorporates repeated interaction-induced scattering between two sites which are excluded from the irreducible self-energy but need to be accounted for in the lattice Dyson equation (2). An important point concerns the incorporation of the explicit hopping between nearest neighbor sites  $t(\underline{a})$ . In the present approach the single-particle transfers and free propagations through the medium are explicitly separated from correlation effects in both models, cf. Eqs. (2) and (11). This implies for the two-impurity model the hopping to be incorporated into the effective medium [see Eqs. (11) and (15)] and ensures translational invariance. Additionally, any imbalance in the treatment of inter- and intra-cluster hopping in the two-impurity model, as it occurs, for instance, in the CDMFT, is removed.

### III. SELF-CONSISTENT SCHEME APPLIED TO THE 2d-HUBBARD MODEL

In this section we present results for the two-dimensional ( $d = 2$ ) Hubbard model (1) obtained with the approximation scheme described in the previous section. We focus on the metallic regime at not too low temperatures. Long-ranged magnetic order and superconducting states are thus excluded, whereas magnetic correlations of finite extent and the precursor regime of a metal-insulator transition are included and accessible.

For the solution of the two-impurity problems we employ a solver based on direct perturbation theory in the hybridization<sup>11,32</sup> which is an extension of the two-orbital solver<sup>33</sup> and which is described elsewhere.<sup>28,34</sup> In contrast to the usual noncrossing approximation<sup>35</sup> (NCA) this two-impurity enhanced noncrossing approximation includes vertex corrections which allow for the accurate description of finite Coulomb repulsions.

An important requirement for the two-impurity solver is, it needs to be able to treat dynamic non-diagonal effective media  $\tilde{T}_{\underline{a}}^{(2\text{imp},\underline{a})}(z)$ .

We study the Hubbard model on a two-dimensional simple-cubic lattice with nearest-neighbor hopping only. The half-bandwidth  $D = 2dt = 4t$  is used as unit of energy and we set  $k_B = c = \hbar = 1$ . The noninteracting spectral function of this system is shown in the inset of Fig. 2(a).

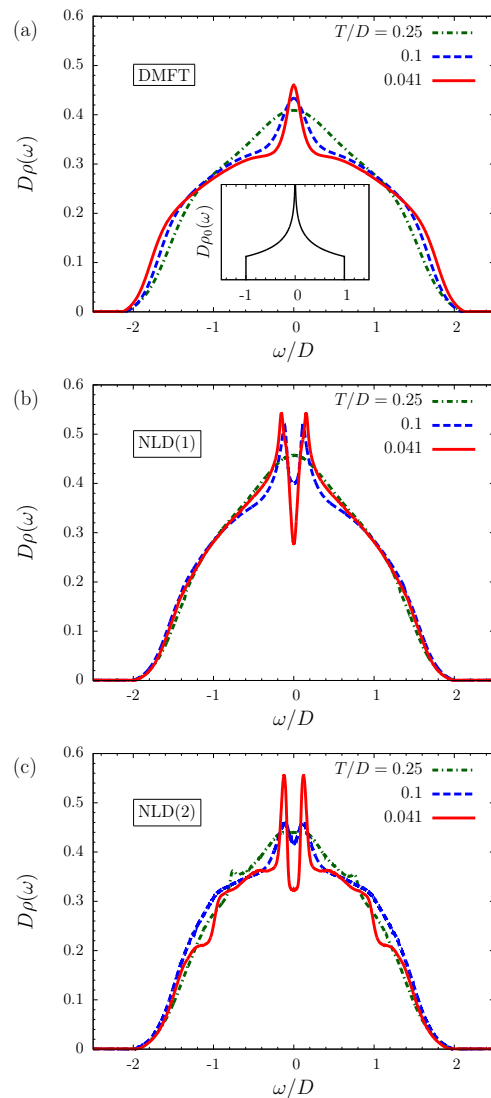


FIG. 2. (Color online) Comparison of the spectral function of the two-dimensional ( $d = 2$ ) half-filled Hubbard model on a simple cubic lattice for various temperatures  $T$  and for different levels of the nonlocal approximation: (a) DMFT, (b) NLD(1), (c) NLD(2). The parameters in all calculations are  $U/D = 1$  and  $\epsilon = -\frac{U}{2} = -\frac{D}{2}$ . All curves are calculated with the two-impurity enhanced noncrossing approximation as impurity solver. The inset in panel (a) shows the noninteracting density of states.

In order to investigate the influence of the nonlocal correlations we consider various stages of the scheme differing in the maximum distance  $\|\underline{a}\|$  to be incorporated into the approximation. This distance is measured with a Manhattan metric indicated by  $\|\cdot\|$  reflecting the minimum number of elementary hoppings between the two sites. For example, the approximation denoted with NLD(1) includes only two-impurity models of nearest-neighbor lattice sites, that is, the set of distance vectors is given by  $\underline{a}_1 \in \{(\pm 1, 0)^T, (0, \pm 1)^T\}$ . Accordingly, in NLD(2) this set is augmented with the four



next-nearest neighbor distances, i.e. the set of vectors is  $\underline{a}_2 \in \{\underline{a}_1, (\pm 1, \pm 1)^T, (\pm 2, 0)^T, (0, \pm 2)^T\}$  and so on.

Figure 2 displays the local single-particle spectral function

$$\rho(\omega) = -\frac{1}{\pi} \text{Im} \frac{1}{N} \sum_{\underline{k}} G_{\underline{k}}(\omega + i0^+) \quad (24)$$

for three different temperatures and various stages of the approximation. Panel (a) shows the usual DMFT solution, while panels (b) and (c) show the NLD(1) and NLD(2) spectral functions, respectively. The sequence of decreasing temperatures reveals the development of the well known many-body resonance at the Fermi level  $\mu = \omega = 0$  in DMFT [panel (a)] indicating the formation of low-energy quasiparticles.<sup>16</sup>

The inclusion of nonlocal correlations by utilizing NLD(1) leads to the formation of a pseudogap inside this resonance [see panels (b)]. A further inclusion of next-nearest neighbor correlations [panel (c)] the gap widens and the sidepeaks become more pronounced. We cannot definitely decide whether or not a complete gap forms at zero temperature ( $T \rightarrow 0$ ) where the spectral function vanishes at the Fermi energy, as it was found in a recent two-site DCA calculation.<sup>36</sup> Too low temperatures can not be investigated with our impurity solver due to the violation of Fermi liquid properties.<sup>28,37</sup>

Additionally, in the high-energy part of the spectrum the inclusion of additional neighbors seems to bring out more of the van-Hove singularities at  $\omega = \pm D$  of the original unperturbed ( $U = 0$ ) spectrum [see inset of Fig. 2(a)].

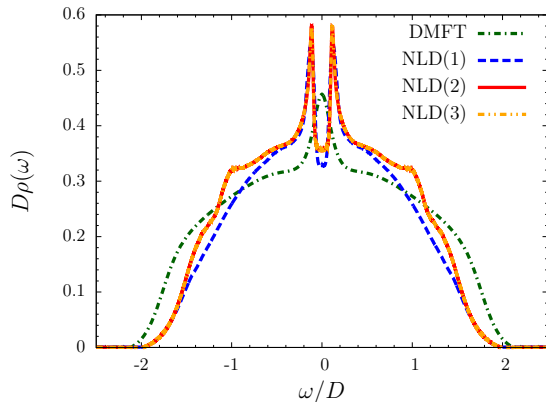


FIG. 3. (Color online) Comparison of the spectral function for the different levels of the NLD(i) approximation. The two-site correlations included range from between nearest neighbor sites in NLD(1) up to all pairs of sites reachable by three elementary hoppings NLD(3). Other parameters are as in Fig. 2.

Inclusion of additional sites with  $\|\underline{a}\| > 2$  into our NLD-scheme does not produce considerable changes, at least for this choice of parameters. This can be observed in Fig. 3, where spectral functions for a fixed temperature  $T = 0.05D$  are shown for various maximal distances

up to  $\|\underline{a}\| = 3$ , i.e. including neighbors reachable by up to three transfer processes  $\sim t$ . The changes become successively smaller and the curves from NLD(2) and NLD(3) are already almost indistinguishable.

Our calculations clearly show the appearance of high sidepeaks at the borders of the pseudogap. The existence of sidepeaks in the low-energy spectrum is in accord with numerical DCA results,<sup>20</sup> where, however, large cluster sizes were necessary to resolve gap and sidepeaks.

We would like to point out, that the sidepeaks in the low-lying quasiparticle regime bear a strong resemblance to what is observed in a related work<sup>28</sup> for the TIAM. In our opinion we now find a coherent version of the splitting-scenario described there: The direct and the induced effective hopping generate bonding and antibonding molecular-like orbitals amongst different sites. The strength of this strongly depends on the crystal structure since the relevant effective matrix elements vary and oscillate with distance.<sup>28</sup> They are also very sensitive to the position of the Fermi level, which sets a scale for such oscillations. The phase-information and coherence of electron propagations which is necessary for such a splitting is fully incorporated into our approach according to Eq. (21).

These aspects also manifest themselves in the sharpening of the high-energy features around  $\omega \approx D$  when going from NLD(1) to NLD(2,3).

In addition to the bonding-antibonding splitting, an effective antiferromagnetic exchange  $J_t = \frac{4t^2}{U}$  between neighboring sites is generated which leads to the suppression of Kondo-like correlations. Both effects described above induce a pseudogap and can lead to a splitting of the coherent many-body resonance at the Fermi level. These cases could in principle be distinguished as the splitting due to molecular binding should be linear in  $|t|$ , while the magnetic singlet-triplet splitting  $J_t$  is proportional to  $t^2$ . However, our choice of parameter values implies similar magnitudes for the hopping  $t$  and the effective exchange  $J_t$ , and both effects should be of comparable size here.

An interesting question is, whether the excitations in the vicinity of the Fermi surface form a dispersive band or are narrowly concentrated in  $\underline{k}$ -space. We show in Fig. 4 the  $\underline{k}$ -resolved spectral function

$$\rho(\underline{k}, \omega) = -\frac{1}{\pi} \text{Im} G_{\underline{k}}(\omega + i0^+) \quad (25)$$

for  $\underline{k}$  along the diagonal (1,1)-direction in the Brillouin zone. One still recognizes the original cosine-form of a tight-binding band via the positions of the peaks in the projection onto the  $k - \omega$ -plane. However, these peaks develop a considerable width with growing  $|\omega|$ , which indicates that quasiparticle excitations are not well defined away from the Fermi surface. Near the Fermi level  $\omega = 0$  two distinct pairs of narrow peaks are visible at wave-vectors  $\underline{k} \approx \pm \frac{\pi}{2}(1,1)^T$ . Even though very slight remnants of these peaks are observable at neighboring wave vectors too, their height is rapidly suppressed as  $\underline{k}$  moves

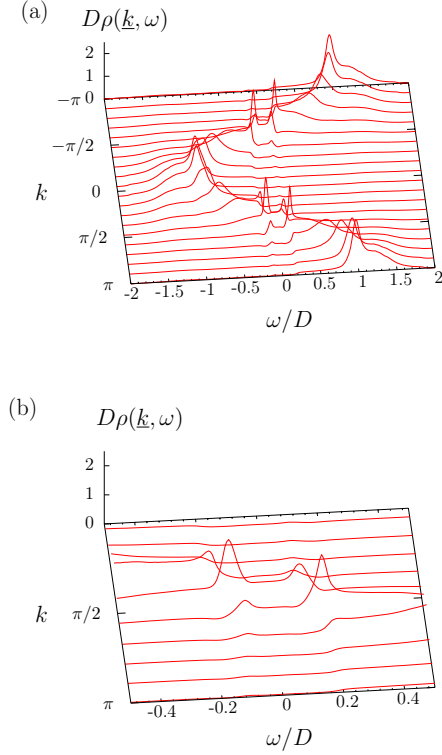


FIG. 4. (Color online)  $\underline{k}$ -resolved spectral function obtained with the NLD(2) for wave vectors along the (1,1)-direction, and for  $\epsilon/D = -\frac{1}{2}$ ,  $U/D = 1$  and  $T/D = 0.05$ . Panel (a) shows the full energy interval while panel (b) displays a magnification of the energy interval around the Fermi-energy.

away from  $\pm\frac{\pi}{2}(1,1)^T$ . Since these maxima apparently furnish the spectral weight of the flanks of the pseudogap observable, e.g., in Fig 3, we conclude those side-peaks to be rather localized in  $\underline{k}$ -space. Thus, they are a result of increasing lattice coherence at decreasing temperature.

Remarkably, also near the band edges at  $\underline{k} = \underline{0}$  and  $\underline{k} = \pm\pi(1,1)^T$  with respective energies  $\omega \approx \pm D$  rather narrow peaks appear on top of the broad resonances connected with the original band. Since they show up only if next-nearest neighbors are included, i.e. in NLD(2) but not in NLD(1) (and DMFT), we attribute them to next-nearest neighbor correlations, possibly of magnetic nature. A participation of an indirect binding effect due to the repeated action of the transfer  $t$ , i.e. a molecular orbital-like effect, can also not be excluded with our choice of parameters.

Up to now a symmetric situation  $2\epsilon + U = 0$  was investigated, in which a possible Mott-Hubbard gap as well as a possible pseudogap in the low-energy quasiparticle regime both were to open around the Fermi-level. Both effects can be separated and identified individually by moving away from half-filling, i.e. with increasing doping. Equivalently, we increase the Coulomb-repulsion  $U$  beyond the value  $U = -2\epsilon$  and keep all other parameters

fixed.

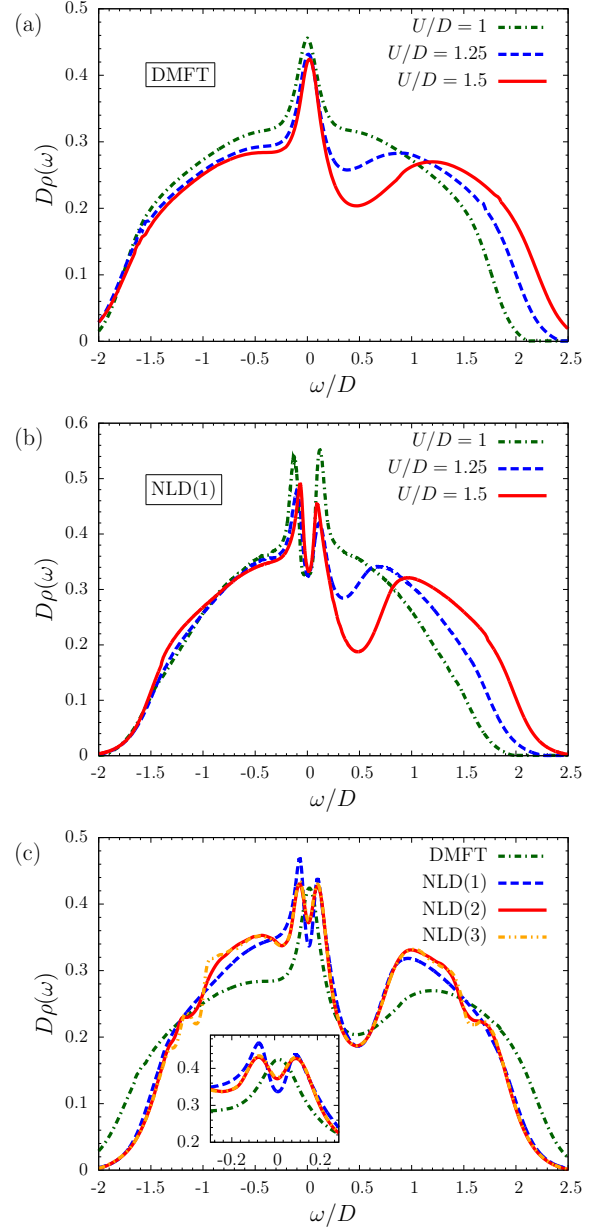


FIG. 5. (Color online) Spectral functions for fixed  $\epsilon = -\frac{D}{2}$  and temperature  $T/D = 0.05$  for various  $U$ . (a) DMFT (b) NLD(1). (c) Spectral function for fixed  $U/D = 1.5$  and different stages of the approximation as indicated. The inset shows a close up of the low-energy region around the Fermi level. The fillings corresponding to the curves shown in (c) are  $n_{\text{DMFT}} \approx 0.90$  and  $n_{\text{NLD}(i)} \approx 0.92$ .

Calculations for such particle-hole asymmetric situations are shown in Fig. 5. Panel (a) displays the formation of a Mott-Hubbard gap at positive energies with increasing  $U$  as calculated with the DMFT-approximation. As expected, the center of the incipient gap moves away from the Fermi level by an amount proportional to  $U$  while the many-body resonance remains pinned at the

Fermi level.

Figure 5(b) shows results of NLD(1)-calculations for the same values of  $U$ . The Mott-Hubbard gap forms at positive energies in a similar fashion as in the DMFT-results of panel (a). Additionally, a pseudogap emerges in the many-body resonance at the Fermi level as it was already found in earlier work.<sup>20–24,38</sup>

The last part (c) of Fig. 5 shows the effect of including more neighbors in our NLD( $i$ )-scheme for fixed Coulomb interaction  $U$ . One again recognizes the dominant role of nearest-neighbor correlations since the spectra with  $i \geq 1$  all differ considerably from the DMFT-result. The low-energy region seems to be converged for  $i = 2$ , and the inclusion of next-nearest neighbors apparently smoothens the spikes around the pseudogap.

In contrast, the inclusion of next-next-nearest neighbors ( $i = 3$ ) still has considerable impact on the high-energy features at negative energies while at positive energies only small differences are induced. This apparently indicates a reduced hybridization and corresponding band narrowing for states in the vicinity of the negative band edge. The importance of lattice structure, coherence and correlations for the possible development of hybridization gaps and band splittings as they were already discussed in the symmetric case is evident from these results.

The longer-ranged correlations also seem to work in favor of restoring particle-hole symmetry in the low-energy region [see inset of Fig. 5(c)], a phenomenon which is also discussed in connection with the cuprate superconductors.<sup>23,24,39</sup>

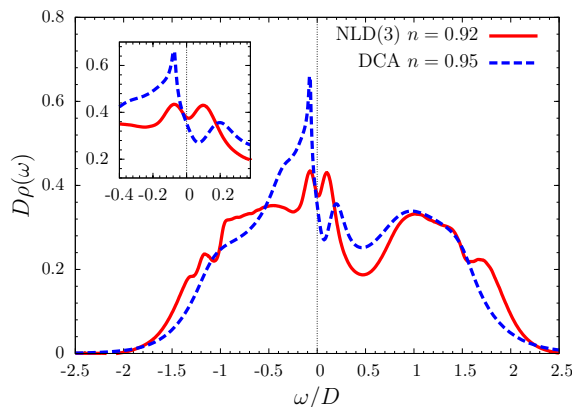


FIG. 6. (Color online) Comparison of NLD(3) and DCA spectral functions. The NLD(3) curve is the one shown in Fig. 5(c). The DCA result is taken from Fig. 5 of Ref. 24 and was obtained from self-consistent quantum Monte Carlo solution of a 16-site cluster for  $U/D = 1.5$  and  $T/D = 0.017$ . The filling for the DCA calculation of  $n_{\text{DCA}} \approx 0.95$  is slightly larger than the NLD(3) filling,  $n_{\text{NLD}(3)} \approx 0.92$ . The inset shows an enlargement of the region around the Fermi level.

Figure 6 compares a NLD(3) spectral function for finite doping and  $U = 1.5D$  with a spectrum obtained from a DCA calculation as it was published in Fig. 5 of Ref. 24.

The qualitative features of both approaches nicely agree: the humps and minima visible in the DCA spectra translate to corresponding but more pronounced features in the NLD(3). Given the different nature of the two approximations, this provides additional evidence for the physical nature of the observed structures.

The magnitude of the pseudogap is of the same order in both approaches, although the DCA result is slightly larger and the low-energy spectrum much more asymmetric. One reason for this can be found in the enhanced two-impurity noncrossing approximation as the two-impurity solver, which is known to produce a too small many-body low-energy scale for the SIAM. This is especially relevant for the low-energy region and also translates to self-consistent approximations (see, e.g. Ref. 15).

The different temperatures of both calculations should not be relevant for the qualitative features as  $T$  is already rather low and further decreasing it will only slightly deepen the pseudogap.

However, a qualitative difference between the two calculations is found in the different fillings which in general strongly influences the low-energy spectral function. The analysis in Ref. 24 revealed that decreasing the filling from  $n_{\text{DCA}} \approx 0.95$  to  $n_{\text{DCA}} \approx 0.88$  (for otherwise identical parameters) leads to a spectral function which is nearly particle-hole symmetric at low energies and does not exhibit a pseudogap. In this light, the NLD(3) spectral function for  $n_{\text{NLD}(3)} \approx 0.92$  with a nearly symmetric low-energy spectrum and a small pseudogap represent a plausible intermediate solution.

#### IV. CONCLUSION

We have proposed a novel general and nonperturbative scheme for the treatment of correlated electron systems on crystal lattices. Our approach represents an extension of the well-known DMFT to include nonlocal two-site correlations with arbitrary spatial extent.

The self-consistent formulation establishes a mapping between nonlocal two-site correlations of the lattice model and the equivalent functions of various two-impurity Anderson models with varying distance. The two-impurity models are solved in real-space, but the extracted correlation functions are transformed into momentum space via a Fourier transform. Thereby translational invariance is built into our scheme by construction.

Most important, the spatial range of correlations which are explicitly included in the treatment is unrestricted in principle. It corresponds to the maximum impurity-impurity distance in an effective TIAM which is solved in our approach, and is therefore only limited by the accuracy of the two-impurity solver.

As a first application, we applied our scheme to the Hubbard model on a two-dimensional simple-cubic lattice. We found that the leading nonlocal correlations produce a pseudogap in the low-energy single-particle excitation spectrum as it is to be expected.<sup>20–24,38</sup> Moreover,



pronounced side-peaks occur as a signature of increasing coherence. In a situation without particle-hole symmetry we could clearly discriminate between the Mott-Hubbard gap induced by mostly local atomic correlations and the pseudogap, which is found in the many-body resonance at the Fermi level. We have also demonstrated that the inclusion of correlations over larger distances brings out more details of the excitation spectra in the high-energy region.

Additionally, our method compares very well to results from the DCA. The spectral functions of both approaches exhibit similar qualitative features for finite doping, although they are more pronounced in our scheme. Also, the pseudogap obtained within both approaches is of the same magnitude.

Thus, the scheme presented opens an excellent perspective for more detailed investigations of systems where nonlocal correlations play an important role. These include phase transitions and critical phenomena in general, and quantum critical points in particular, as they are found, for example, in heavy fermion compounds or

cuprate superconductors.

Also, the calculation of nontrivial critical exponents and their scaling behavior<sup>40</sup> seems to be in reach using this new approach. In some cases it will nevertheless be necessary to include higher-order irreducible correlations beyond those between only two sites. This will be of particular importance, when complicated ground states involving correlations on plaquettes of sites or general resonating valence bond-states are under consideration.<sup>41</sup>

## ACKNOWLEDGMENTS

We thank Eberhard Jakobi for fruitful discussions, Kuang-Shing Chen for providing us with the DCA data shown in Fig. 6, and the NIC, Forschungszentrum Jülich, for their supercomputer support under Project No. HDO00. SS acknowledges financial support from the Deutsche Forschungsgemeinschaft under Grant No. AN 275/6-2.

- 
- \* Email: sebastian.schmitt@tu-dortmund.de
- <sup>1</sup> P. Coleman, Ann. Henri Poincaré, Suppl. 2 **4**, S559 (2003).
  - J. Quintanilla and C. Hooley, Physics World **22**, 32 (2009).
  - <sup>2</sup> T. V. Ramakrishnan, Current Science **95**, 1284 (2008).
  - <sup>3</sup> N. Plakida, *High-Temperature Cuprate Superconductors*, vol. 166 of *Springer Series in solid-state sciences* (Springer, 2010).
  - <sup>4</sup> C. Lacroix, P. Mendels, and F. Mila, eds., *Introduction to Frustrated Magnetism*, vol. 164 of *Springer Series in Solid-State Sciences* (Springer, 2011).
  - <sup>5</sup> N. Grewe and F. Steglich, *Handbook on the Physics and Chemistry of Rare Earths* (North-Holland, 1991), vol. 14, p. 343.
  - P. Coleman, *Handbook of Magnetism and Advanced Magnetic Materials* (John Wiley and Sons, Ltd., Weinheim, 2007), vol. 1, chap. Heavy Fermions: electrons at the edge of magnetism, pp. 95–148.
  - <sup>6</sup> M. R. Norman, D. Pines, and C. Kallin, Adv. Phys. **54**, 715 (2005).
  - <sup>7</sup> M. Vojta, Nat. Phys. **5**, 623 (2009).
  - <sup>8</sup> P. B. Wiegmann and A. M. Tsvelick, J. Phys. C **16**, 2281 (1983).
  - A. M. Tsvelick and P. B. Wiegmann, J. Phys. C **16**, 2321 (1983).
  - N. Andrei, K. Furuya, and J. H. Lowenstein, Rev. Mod. Phys. **55**, 331 (1983).
  - <sup>9</sup> A. C. Hewson, *The Kondo Problem to Heavy Fermions* (Cambridge University Press, Cambridge, 1993).
  - <sup>10</sup> K. G. Wilson, Rev. Mod. Phys. **47**, 773 (1975).
  - R. Bulla, T. Costi, and T. Pruschke, Rev. Mod. Phys. **80**, 395 (2008).
  - J. E. Hirsch and R. M. Fye, Phys. Rev. Lett. **56**, 2521 (1986).
  - P. Werner, A. Comanac, L. de' Medici, M. Troyer, and A. J. Millis, Phys. Rev. Lett. **97**, 076405 (2006).
  - S. R. White, Phys. Rev. Lett. **69**, 2863 (1992).
  - <sup>11</sup> N. Grewe, S. Schmitt, T. Jabben, and F. B. Anders, J. Phys.: Condens. Matter **20**, 365217 (2008).
  - <sup>12</sup> N. Grewe, Solid State Commun. **50**, 19 (1984).
  - N. Grewe, Z. Phys. B **52**, 193 (1983).
  - N. Grewe, Z. Phys. B **67**, 323 (1987).
  - Y. Kuramoto, in *Theory of heavy fermions and valence fluctuation*, edited by T. Kasuka and T. Saso (Springer, Berlin, 1985), vol. 62 of *Springer series in solid state sciences*, pp. 152–161.
  - <sup>13</sup> T. Pruschke, M. Jarrell, and J. Freericks, Adv. Phys. **44**, 187 (1995).
  - A. Georges, G. Kotliar, W. Krauth, and M. J. Rozenberg, Rev. Mod. Phys. **68**, 13 (1996).
  - A. Georges, in *Lectures on the physics of highly correlated electron systems VIII*, edited by A. Avella and F. Mancini (2004), vol. 715 of *AIP Conf. Proc.*, pp. 3–74.
  - D. Vollhardt, Ann. Phys. (Berlin) pp. 1–23 (2011).
  - <sup>14</sup> T. Pruschke and R. Peters, J. Magn. Magn. Mater. **310**, 935 (2007).
  - G. Sordi, A. Amaricci, and M. J. Rozenberg, Phys. Rev. Lett. **99**, 196403 (2007).
  - K. Held and R. Bulla, Eur. Phys. J. B **17**, 7 (2000).
  - T. Pruschke, R. Bulla, and M. Jarrell, Phys. Rev. B **61**, 12799 (2000).
  - R. Bulla, Phys. Rev. Lett. **83**, 136 (1999).
  - <sup>15</sup> A. Y. Matsuura, H. Watanabe, C. Kim, S. Doniach, Z.-X. Shen, T. Thio, and J. W. Bennett, Phys. Rev. B **58**, 3690 (1998).
  - G. Kotliar and D. Vollhardt, Physics Today **57**, 53 (2004).
  - K. Maiti, R. S. Singh, and V. R. R. Medicherla, Phys. Rev. B **76**, 165128 (2007).
  - P. Grete, S. Schmitt, C. Raas, F. B. Anders, and G. S. Uhrig, Phys. Rev. B **84**, 205104 (2011).
  - S. Schmitt, Phys. Rev. B **82**, 155126 (2010).
  - <sup>16</sup> N. Grewe, Ann. Phys. (Leipzig) **14**, 611 (2005).
  - <sup>17</sup> V. Zlatić and B. Horvatic, Solid State Commun. **75**, 263 (1990).

- M. Jarrell, Phys. Rev. Lett. **69**, 168 (1992).  
M. Jarrell, Phys. Rev. B **51**, 7429 (1995).  
J. Kuneš, Phys. Rev. B **83**, 085102 (2011).  
S. Schmitt, Ph.D. thesis, TU Darmstadt (2009), available at <http://tuprints.ulb.tu-darmstadt.de/1264/>.  
S. Schmitt, N. Grewe, and T. Jabben, Phys. Rev. B **85**, 024404 (2012).
- <sup>18</sup> G. R. Stewart, Rev. Mod. Phys. **73**, 797 (2001).  
G. R. Stewart, Rev. Mod. Phys. **78**, 743 (2006).  
Q. Si and F. Steglich, Science **329**, 1161 (2010).  
H. v. Lohneysen, A. Rosch, M. Vojta, and P. Wolfle, Rev. Mod. Phys. **79**, 1015 (2007).  
S. Sachdev, Phys. Status Solidi B **247**, 537 (2010).  
D. M. Broun, Nature Physics **4**, 170 (2008).
- <sup>19</sup> T. Maier, M. Jarrell, T. Pruschke, and M. H. Hettler, Rev. Mod. Phys. **77**, 1027 (2005).  
J. L. Smith and Q. Si, Phys. Rev. B **61**, 5184 (2000).  
A. Toschi, A. A. Katanin, and K. Held, Phys. Rev. B **75**, 045118 (2007).  
A. A. Katanin, A. Toschi, and K. Held, Phys. Rev. B **80**, 075104 (2009).  
A. N. Rubtsov, M. I. Katsnelson, and A. I. Lichtenstein, Phys. Rev. B **77**, 033101 (2008).  
A. N. Rubtsov, M. I. Katsnelson, A. I. Lichtenstein, and A. Georges, Phys. Rev. B **79**, 045133 (2009).  
A.-M. Tremblay, *Theoretical methods for Strongly Correlated Systems* (Springer Verlag, 2012), chap. Two-Particle-Self-Consistent Approach for the Hubbard Model.
- <sup>20</sup> C. Huscroft, M. Jarrell, T. Maier, and A.-N. Tahvildarzadeh, Phys. Rev. Lett. **86**, 139 (2001).  
S. Moukouri and M. Jarrell, Phys. Rev. Lett. **87**, 167010 (2001).  
M. Jarrell, T. Maier, C. Huscroft, and S. Moukouri, Phys. Rev. B **64**, 195130 (2001).
- <sup>21</sup> Y. M. Vilk, Phys. Rev. B **55**, 3870 (1997).  
D. J. Scalapino, *Handbook of High Temperature Superconductivity* (Springer, Berlin, 2007), chap. Numerical Studies of the 2D Hubbard Model, p. 495.  
B. Kyung, S. S. Kancharla, D. S  n  chal, A.-M. S. Tremblay, M. Civelli, and G. Kotliar, Phys. Rev. B **73**, 165114 (2006).  
A.-M. S. Tremblay, B. Kyung, and D. S  n  chal, Low Temp. Phys. **32**, 424 (2006).
- <sup>22</sup> A. Macridin, M. Jarrell, T. Maier, P. R. C. Kent, and E. D'Azevedo, Phys. Rev. Lett. **97**, 036401 (2006).
- <sup>23</sup> N. S. Vidhyadhiraja, A. Macridin, C. Sen, M. Jarrell, and M. Ma, Phys. Rev. Lett. **102**, 206407 (2009).  
E. Khatami, K. Mielsons, D. Galanakis, A. Macridin, J. Moreno, R. T. Scalettar, and M. Jarrell, Phys. Rev. B **81**, 201101 (2010).  
S.-X. Yang, H. Fotso, S.-Q. Su, D. Galanakis, E. Khatami, J.-H. She, J. Moreno, J. Zaanen, and M. Jarrell, Phys. Rev. Lett. **106**, 047004 (2011).
- <sup>24</sup> K.-S. Chen, S. Pathak, S.-X. Yang, S.-Q. Su, D. Galanakis, K. Mielsons, M. Jarrell, and J. Moreno, Phys. Rev. B **84**, 245107 (2011).
- <sup>25</sup> G. Kotliar, S. Y. Savrasov, G. P  lsson, and G. Biroli, Phys. Rev. Lett. **87**, 186401 (2001).  
G. Biroli, O. Parcollet, and G. Kotliar, Phys. Rev. B **69**, 205108 (2004).
- <sup>26</sup> M. H. Hettler, A. N. Tahvildar-Zadeh, M. Jarrell, T. Pruschke, and H. R. Krishnamurthy, Phys. Rev. B **58**, R7475 (1998).  
M. H. Hettler, M. Mukherjee, M. Jarrell, and H. R. Krishnamurthy, Phys. Rev. B **61**, 12739 (2000).
- <sup>27</sup> A. Isidori and M. Capone, Phys. Rev. B **79**, 115138 (2009).
- <sup>28</sup> T. Jabben, N. Grewe, and S. Schmitt, Phys. Rev. B **85**, 045133 (2012).
- <sup>29</sup> J. Hubbard, Proc. Roy. Soc. A **276**, 238 (1963).
- <sup>30</sup> S. Alexander and P. W. Anderson, Phys. Rev. **133**, A1594 (1964).
- <sup>31</sup> A. Schiller and K. Ingersent, Phys. Rev. Lett. **75**, 113 (1995).
- <sup>32</sup> H. Keiter and J. C. Kimball, Phys. Rev. Lett. **25**, 672 (1970).  
N. Grewe and H. Keiter, Phys. Rev. B **24**, 4420 (1981).  
H. Keiter and G. Morandi, Phys. Rep. **109**, 227 (1984).
- <sup>33</sup> N. Grewe, T. Jabben, and S. Schmitt, Eur. Phys. J. B **68**, 23 (2009).
- <sup>34</sup> T. Jabben, Ph.D. thesis, TU Darmstadt (2010).
- <sup>35</sup> N. Grewe, Z. Phys. B **53**, 271 (1983).  
Y. Kuramoto, Z. Phys. B **53**, 37 (1983).  
N. E. Bickers, Rev. Mod. Phys. **59**, 845 (1987).
- <sup>36</sup> T. Pruschke, Physica B **359-361**, 633 (2005).
- <sup>37</sup> S. Schmitt, T. Jabben, and N. Grewe, Phys. Rev. B **80**, 235130 (2009).
- <sup>38</sup> N. Lin, E. Gull, and A. J. Millis, Phys. Rev. B **82**, 045104 (2010).  
T. D. Stanescu, M. Civelli, K. Haule, and G. Kotliar, Ann. Phys. **321**, 1682 (2006).  
T. Maier, M. Jarrell, T. Pruschke, and J. Keller, Eur. Phys. J. B **13**, 613 (2000).
- <sup>39</sup> S. Chakraborty, D. Galanakis, and P. Phillips, Phys. Rev. B **82**, 214503 (2010).
- <sup>40</sup> G. Rohringer, A. Toschi, A. Katanin, and K. Held, Phys. Rev. Lett. **107**, 256402 (2011).
- <sup>41</sup> H.-Y. Yang, A. M. L  uchli, F. Mila, and K. P. Schmidt, Phys. Rev. Lett. **105**, 267204 (2010).  
Z. Y. Meng, T. C. Lang, S. Wessel, F. F. Assaad, and A. Muramatsu, Nature **464**, 847 (2010).  
S. Yan, D. A. Huse, and S. R. White, Science **332**, 1173 (2001).